Elucidation of Structure and Location of V(IV) Ions in Heteropolyacid Catalysts $H_4PVMo_{11}O_{40}$ as Studied by Hyperfine Sublevel Correlation Spectroscopy and Pulsed Electron Nuclear Double Resonance at W- and X-Band Frequencies

Andreas Pöppl,*,† Palanichamy Manikandan,‡ Klaus Köhler,§ Peter Maas,§ Peter Strauch,|| Rolf Böttcher,† and Daniella Goldfarb‡

Contribution from the Universität Leipzig, Fakultät für Physik und Geowissenschaften, Linnéstrasse 5, D-04103 Leipzig, Germany, The Weizmann Institute of Science, Rehovot, Israel, 76100, Anorganisch-chemisches Institut, Technische Universität München, Lichtenbergstrasse 4, D-85747 Garching, Germany, and Universität Potsdam, Institut für Anorganische Chemie und Didaktik der Chemie, Postfach 60 15 53, D-14415 Potsdam, Germany

Received December 19, 2000. Revised Manuscript Received February 21, 2001

Abstract: Electron spin resonance, pulsed electron nuclear double resonance (ENDOR) spectroscopy at W- and X-band frequencies, and hyperfine sublevel correlation (HYSCORE) spectroscopy have been employed to determine the location of the V(IV) ions in $H_4PVMo_{11}O_{40}$ heteropolyacid catalysts. In these materials the heteropolyanions have the well-known structure of the Keggin molecule. Interactions of the unpaired electrons of the paramagnetic vanadyl ions (VO^{2+}) with all relevant nuclei (^1H, ^{31}P, and ^{51}V) could be resolved. The complete analysis of the hyperfine coupling tensor for the phosphorus nucleus in the fourth coordination sphere of the V(IV) ion allowed for the first time a detailed structural analysis of the paramagnetic ions in heteropolyacids in hydrated and dehydrated catalysts. The ^{31}P and ^1H ENDOR results show that V(IV) ions are incorporated as vanadyl pentaaqua complexes $[VO(H_2O)_5]^{2+}$ in the void space between the heteropolyanions in the hydrated heteropolyacid. For the dehydrated $H_4PVMo_{11}O_{40}$ materials the distance between the V(IV) ion and the central phosphorus atom of the Keggin molecule could be determined with high accuracy on the basis of orientation-selective ^{31}P ENDOR experiments and HYSCORE spectroscopy. The results give a first direct experimental evidence that the paramagnetic vanadium species are not incorporated at molybdenum sites into the Keggin structure of $H_4PVMo_{11}O_{40}$ and also do not act as bridges between two Keggin units after calcination of the catalyst. The vanadyl species are found to be directly attached to the Keggin molecules. The VO^{2+} ions are coordinated to four or three outer oxygen atoms from one $PVMo_{11}O_{40}^{-4}$ heteropolyanion in a trigonal-pyramidal or slightly distorted square-pyramidal coordination geometry, respectively.

1. Introduction

Heteropolyacids[1] (HPA) ($H_3PMo_{12}O_{40}$) of the Keggin type[2] and their salts are efficient heterogeneous catalysts for the selective oxidation of alkanes and aldehydes.[3−5] The catalytic performance of the HPA can be enhanced by an incorporation of V(V) into the Keggin heteropolyanion.[6,7] Therefore, the location and coordination geometry of the vanadium ions in hydrated and particularly in dehydrated $H_4PVMo_{11}O_{40}$ materials are of importance for the elucidation of the catalytic behavior and the thermal stability of the HPA catalysts. It has been reported that a fraction of the introduced vanadium is always present as paramagnetic vanadyl V(IV) ions[8,9] which can be characterized by a variety of electron spin resonance (ESR) techniques. Although a series of papers report on V(IV) ESR studies of HPA materials,[8−12] conclusive experimental evidence for the location of the paramagnetic vanadium species at either molybdenum sites in the Keggin unit or at interstitial lattice sites in the void space between the anionic Keggin molecules is still lacking. The study of the paramagnetic vanadium valence states seems to be particularly important because the majority of the vanadium ions have been found to be in the V(IV) state during and after catalytic reactions[9,11] or after reduction by organic reactants,[12] suggesting a specific role of the V(IV) ions in the catalytic cycle of the HPA systems.

† Universität Leipzig.
‡ The Weizmann Institute of Science.
§ Technische Universität München.
|| Universität Potsdam.

(1) Pope, M. T.; Müller, A. *Angew. Chem.* **1991**, *103*, 56.
(2) Keggin, J. F. *Proc. R. Soc.* **1934**, *A 144*, 75.
(3) Kozhevnikov, I. V. *Catal. Rev. Sci. Eng.* **1995**, *37*, 311.
(4) Okuhura, T.; Mizuno, N.; Misono, M. *Adv. Catal.* **1996**, *41*, 113.
(5) Lee, K.-Y.; Misonso, M., in*Handbook of Heterogeneous Catalysis*; Ertl, G.; Knözinger, H.; Weitkamp, J., Eds.; VCH: Weinheim, 1997, vol. 5, p 118.
(6) Ono, Y. In *Perspectives in Catalysis;* Thomas, J. M., Zamarev, K. I., Eds.; Blackwell: London, 1992.
(7) Mizuno, N.; Misono, M. *J. Mol. Catal.* **1994**, *86*, 319.
(8) Fricke, R.; Jerschkewitz, H.-G.; Öhlmann, G. *J. Chem. Soc., Faraday Trans. 1* **1986**, *82*, 3479.
(9) Aboukaïs, A.; Haubtmann, C.; André, J. J.; Desquilles, C.; Dourdin, M.; Mathes-Juventin-Andrieu, I.; Aïssi, F. C.; Guelton, M. *J. Chem. Soc., Faraday Trans.* **1995**, *91*, 1025.
(10) Bayer, R. Marchal, C.; Liu, F. X.; Tézé, A.; Hervé, G. *J. Mol. Catal. A: Chemical* **1996**, *110*, 65.
(11) Inumaru, K.; Ono, A.; Kubo, H.; Misono, M. *J. Chem. Soc., Faraday Trans. 1* **1998**, *94*, 1765.
(12) Lee, J. K.; Russo, V.; Melsheimer, J.; Köhler, K.; Schlögl, R. *Phys. Chem. Chem. Phys.* **2000**, *2*, 2977.

10.1021/ja004291n CCC: $20.00
Published on Web 04/24/2001

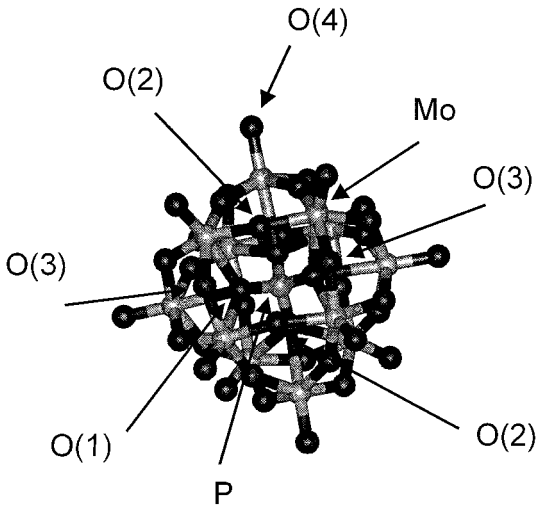

Figure 1. Structure of the $PVMo_{11}O_{40}^{-4}$ heteropolyanion. The vanadium ion is assumed to substitute one of the 12 molybdenum ions in the Keggin molecule.

Heteropolyacids are composed of primary and secondary structures. The most common primary structure of the heteroployacids is the well-known Keggin-type molecule schematically shown in Figure 1. The Keggin structure of the $PVMo_{11}O_{40}^{-4}$ heteropolyanion consists of a central PO_4 tetrahedron which determines the molecular symmetry. The central tetrahedron is surrounded by 12 oxygen octahedra containing the Mo(VI) ions. One of these molybdenum atoms is assumed to be statistically substituted by V(V) ions in $H_4PVMo_{11}O_{40}$ materials. There are four types of oxygen atoms in the Keggin unit. These are the four central oxygen atoms O(1), two types of bridging oxygens O(2) and O(3), each group consisting of 12 oxygens, and finally 12 terminal oxygens O(4). The O(4) atoms form a double bond to the transition metal ions. The bridging and the central oxygens form single bonds to two different metal ions and between the central phosphorus atom and the metal ions, respectively. HPA crystallize with a large number of water molecules.[13] The net negative charge of the $PVMo_{11}O_{40}^{-4}$ heteropolyanion is compensated by either cations or protons/$H_5O_2^+$ to form the secondary structure with the Keggin units at the lattice positions.[14,15] The type of secondary structure of the HPA strongly depends on the number of water molecules of crystallization. In the case of $H_4PVMo_{11}O_{40}$ materials stable hydrated compounds with 13−14 H_2O give rise to a triclinic structure at room temperature. Upon heating, the loss of the crystallization water results in an anhydrous phase with a tetragonal lattice between 370 and 620 K.[13,16] The heating process in this temperature range is accompanied by a progressive decrease in the crystallinity of the HPA material.[13] At temperatures above 620 K the HPA starts to decompose as indicated by the appearance of an orthorhombic MoO_3 phase.

ESR studies of the paramagnetic V(IV) state in HPA materials[8−12] showed that the principal values of the electron Zeeman interaction tensor **g** and of the ^{51}V hyperfine (hf) coupling tensor $\mathbf{A^V}$ of the vanadium ions are sensitive to the structural changes of the HPA induced by thermal treatment or catalytic applications. The amount of the paramagnetic species in the dehydrated (calcined) HPA was determined to be 6% of the total vanadium (IV and V) in the material.[12] After catalysis (selective oxidation reactions) as well as after reduction by organic molecules such as methanol, the majority of vanadium is found to be present in the oxidation state +4.[10−12] Different sets of spin Hamiltonian parameters are found for hydrated and anhydrous HPA.[8,10] However, the **g** tensor and ^{51}V hf coupling data are not sensitive to changes in the second or even higher coordination spheres of the vanadium ion, and therefore the ESR spectrum cannot be used for the determination of the specific structures of the V(IV) complexes and their location within the HPA materials.

To overcome these limitations of ESR spectroscopy, orientation-selective pulsed electron nuclear double resonance (ENDOR) spectroscopy at W- and X-band frequencies and hyperfine sublevel correlation (HYSCORE) experiments were employed in this work to measure the hf coupling between the V(IV) ions and the central phosphorus atom of the heteropolyanion in $H_4PVMo_{11}O_{40}$ materials in the hydrated state and after thermal treatment in oxygen (calcination). The ^{31}P hf coupling data give direct access to the P−V(IV) distance, which in turn allows the localization of the V(IV) sites in the HPA. While most analytical methods fail to determine the V(IV) environment because of the low crystallinity of the active catalyst[13] or the low vanadium content ($\leq$1 atom per Keggin unit), the combination of sophisticated magnetic resonance techniques applied in this work have been most powerful.

2. Experimental Section

Sample Preparation. The $H_4PVMo_{11}O_{40}$ material was synthesized according to the procedure published by Berndt et al.[14] Stoichiometric quantities of MoO_3 and V_2O_5 were dissolved in diluted phosphoric acid at 363 K for 4 h. The solution was then precipitated by evaporation of water at 333 K and finally dried in air at 383 K for 15 h. The obtained samples are denoted as fresh (hydrated) $H_4PVMo_{11}O_{40}$. Dehydrated (anhydrous) samples were obtained by thermal treatment of the fresh $H_4PVMo_{11}O_{40}$ material at 573 K for 1 h in flowing oxygen (50 mL/min. oxygen:helium = 1:2). After this treatment the samples were immediately transferred in ESR quartz glass tubes and sealed without contact to air and moisture.

Spectroscopic Measurements. Pulsed ENDOR and two-pulse field-swept electron spin−echo (ESE) experiments at W-band (94.9 GHz) were carried out at $T = 4.3$ K on a home-built spectrometer described elsewhere.[17] X-band (9.68 GHz) experiments were performed at $T =$ 6 K on a BUKER ESP 380 spectrometer. For the two-pulse field-swept ESE measurements microwave (mw) pulse lengths of $t_{\pi/2} = 50$ ns for $\pi/2$ pulses and $t_\pi = 100$ ns for π pulses with a pulse delay of $\tau = 300$ ns were used at W-band and $t_{\pi/2} = 100$ ns, $t_\pi = 200$ ns, $\tau = 760$ ns at X-band. The Mims[18] ENDOR sequence was employed with mw pulse lengths of $t_{\pi/2} = 100$ ns for both W- and X-band. The radio frequency (rf) pulse widths were $t_{rf} = 20$ μs (W-band) and $t_{rf} = 10$ μs (X-band). The pulse delay between the first two mw pulses was $\tau = 300$ ns or $\tau = 760$ ns for W- and X-band experiments, respectively.

Two-dimensional (2D) HYSCORE experiments ($\pi/2-\tau-\pi/2-t_1-\pi-t_2-\pi/2-\tau$-*echo*)[19] were performed on an X-band BUKER ESP 380 spectrometer at $T = 6$ K with a pulse delay $\tau = 256$ ns. For the second and fourth mw pulse high turning angle (HTA) pulses[20] have been used with a pulse width of $t_{HTA} = 176$ ns to enhance the weak ^{31}P modulation. The other pulse widths were $t_{\pi/2} = 24$ ns and $t_\pi = 48$ ns. A 170 × 170 2D data matrix was sampled with a dwell time of 24 ns. The echo

(13) Fournier, M.; Feumi-Jantou, C.; Rabia, C.; Hervé, G.; Launay, S. *J. Mater. Chem.* **1992**, *2*, 971.
(14) Berndt, S.; Herein, D.; Zemlin, F.; Beckmann, E.; Weinberg, G.; Schütze, J.; Mestl, G.; Schlögl, R. *Ber. Bunsen-Ges. Phys. Chem.* **1998**, *102*, 763.
(15) Bardin, B. B.; Bordawekar, S. V.; Neurock, M.; Davis, R. J. *J. Phys. Chem.* **1998**, *102*, 10817.
(16) Ilkenhans, Th.; Herzog, B.; Braun, Th.; Schlögl, R. *J. Catal.* **1995**, *153*, 275.
(17) Gromov, I.; Krymov, V.; Manikandan, P.; Arieli, D.; Goldfarb, D. *J. Magn. Reson.* **1999**, *139*, 78.
(18) Mims, W. B. *Proc. R. Soc. London* **1965**, *283*, 452.
(19) Höfer, P.; Grupp, A.; Nebenführ, H.; Mehring, M. *Chem. Phys. Lett.* **1986**, *132*, 279.
(20) Jeschke, G.; Rakhmatullin, R.; Schweiger, A. *J. Magn. Reson.* **1998**, *131*, 261.

Table 1. Spin Hamiltonian Parameters of V(IV) Ions in $H_4PVMo_{11}O_{40}$

sample	species	$g_{\|\|}$[a]	$g_\perp$[a]	$A_{\|\|}^V$[b] (cm^{-1})	$A_\perp^V$[b] (cm^{-1})
fresh[c]	A	1.925	1.970	0.0184	0.0072
dehydrated[d]	B	1.926	1.957	0.0149	0.0038

[a] Estimated error is ±0.002. [b] Estimated error is ±0.0003 cm^{-1}. [c] The line widths in the simulation of the field-swept ESE spectrum recorded at X-band were $\Delta B_{||} = \Delta B_\perp = 1.0$ mT at X-band and $\Delta B_{||} = 7.0$ mT, $\Delta B_\perp = 3.7$ mT at W-band. [d] The line widths in the simulation of the field-swept ESE spectrum recorded at X-band were $\Delta B_{||} = 1.9$ mT, $\Delta B_\perp = 1.9$ mT at X-band and $\Delta B_{||} = 18.0$ mT, $\Delta B_\perp = 20.0$ mT at W-band.

decay was eliminated by a third-order ploynomial baseline correction of the experimental data set in both time domains. 2D FT magnitude spectra were calculated and presented as contour plots.

4. Results

Field-Swept ESE. Two-pulse field-swept ESE spectra of the V(IV) ions in fresh and dehydrated $H_4PVMo_{11}O_{40}$ materials were taken at W- and X-band frequencies. Figure 2a,b illustrates the X- and W-band field-swept ESE spectra of fresh $H_4PVMo_{11}O_{40}$ samples. Both powder spectra can be described by an axially symmetric **g** tensor of the V(IV) ion ($3d^1$, $S = {}^1/_2$) and a likewise axially symmetric hf splitting into eight lines due to the interaction of the unpaired electron with the nuclear spin $I = {}^7/_2$ of the ^{51}V vanadium nucleus. Commonly, this vanadium complex in fresh $H_4PVMo_{11}O_{40}$ materials has been denoted as species A in the literature.[8,10,12] The spin Hamiltonian parameters of species A are summarized in Table 1. The parameters were determined by a simulation of the experimental powder patterns using second-order perturbation theory. In the simulations anisotropic line widths $\Delta B_{xx} = \Delta B_{yy} = 3.7$ mT, $\Delta B_{zz} = 7.0$ mT and $\Delta B_{xx} = \Delta B_{yy} = \Delta B_{zz} = 1.0$ mT were used for W- and X-band spectra, respectively. It is worth noting that the W-band spectrum shows a lower spectral resolution than the X-band spectrum. This is reflected by significantly larger line widths, which were required in the simulations of the W-band data and suggest substantial *g* strain effects.

In two-pulse field-swept ESE spectra of dehydrated $H_4PVMo_{11}O_{40}$ materials (Figure 3) a second V(IV) species B is observed with different spin Hamiltonian parameters. The principal values of the axially symmetric **g** and $\mathbf{A^V}$ tensors of species B were likewise obtained by spectral simulations and are given in Table 1. In the X-band spectrum (Figure 3a) only species B could be observed in dehydrated samples. But the W-band spectrum in Figure 3b shows also minor traces of species A at the outer wings of the signal of species B. The amount of species A was determined by the simulations to be about 15% of the total V(IV) concentration. The evolution of different V(IV) species in dependence on the heat-treatment of HPA is well-known and has been reported in the literature.[8−10,12] In general the spectra of dehydrated materials exhibit larger line widths as indicated by a lower spectral resolution. Again the W-band spectrum displays significantly larger line widths ($\Delta B_{xx} = \Delta B_{yy} = 20.0$ mT, $\Delta B_{zz} = 18.0$ mT) than the X-band experiment ($\Delta B_{xx} = \Delta B_{yy} = \Delta B_{zz} = 1.9$ mT) leading to an almost complete loss of the ^{51}V hf structure in the W-band spectrum of dehydrated $H_4PVMo_{11}O_{40}$ (Figure 3b).

The calculation of the ESR resonance fields as a function of the angle θ between the external magnetic field and the $g_{||}$ axis of the V(IV) **g** tensor is useful for the selection of proper field positions for the orientation selective ENDOR measurements. Such θ versus resonance field plots, calculated from the estimated principal values of the **g** and $\mathbf{A^V}$ tensors of the V(IV) ions in dehydrated $H_4PVMo_{11}O_{40}$, are presented in Figures 3c and d for X- and W-band experiments.

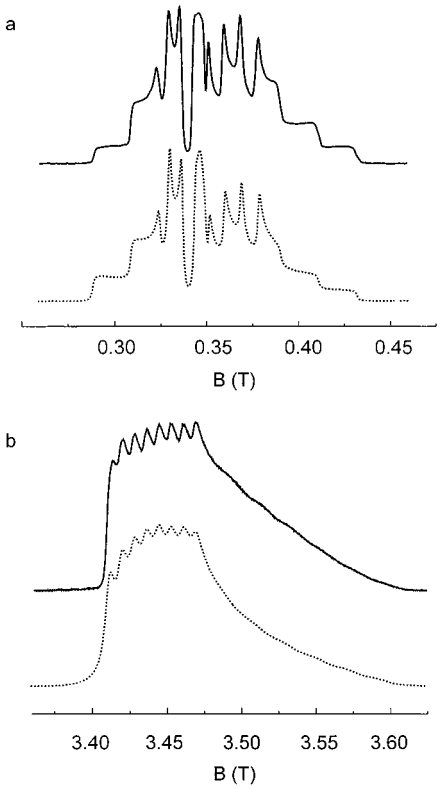

Figure 2. Two-pulse field swept ESE spectra of V(IV) ions in fresh $H_4PVMo_{11}O_{40}$ materials: experimental (solid line) and simulated (dashed line) (a) X-and (b) W-band spectra. Simulation parameters are given in Table 1.

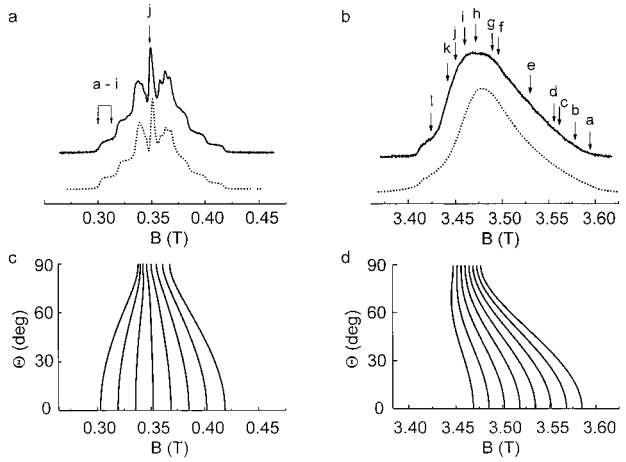

Figure 3. Two-pulse field swept ESE spectra of V(IV) ions in dehydrated $H_4PVMo_{11}O_{40}$ materials: experimental (solid line) and simulated (dashed line) (a) X-and (b) W-band spectra. Calculated magnetic resonance fields in dependence on the angle θ between the external magnetic field and the $g_{||}$ axis of the V(IV) **g** tensor at (c) X- and (d) W-band. Simulation parameters are given in Table 1.

Pulsed ENDOR. X-band pulsed ENDOR spectra of species A and B in fresh and dehydrated $H_4PVMo_{11}O_{40}$ materials are presented in Figure 4. Both spectra show three groups of ENDOR signals at about 3.9, 6.1, and 14.7 MHz. These signals are assigned to weak hf interactions of the paramagnetic V(IV) species with ^{51}V, ^{31}P, and ^1H nuclei based on each of their nuclear Larmor frequencies $\nu_V \approx 4$ MHz, $\nu_P \approx 6$ MHz and $\nu_H \approx 15$ MHz, respectively. The nuclear Larmor frequencies slightly differ between the two spectra since different ESR

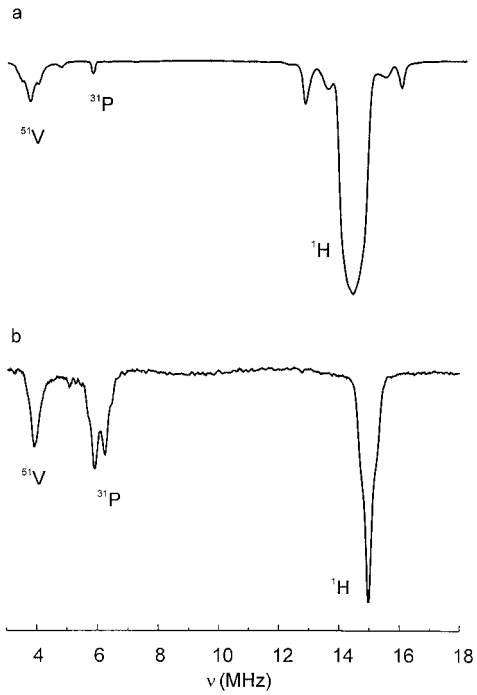

Figure 4. X-band Mims ENDOR spectra of (a) fresh and (b) dehydrated $H_4PVMo_{11}O_{40}$ materials recorded at $B = 0.3349$ and $B = 0.3515$ mT, respectively.

observer fields were used in the two experiments. We have to stress here that the ^{51}V ENDOR signal is not caused by the central ion hf interaction of the V(IV) ion that is already observed in the ESR spectra but must be assigned to weak hf interactions with diamagnetic V(V) species. In both spectra protons give rise to the most intense ENDOR signals but their shape differs between parent and heat-treated samples. Whereas the spectrum of the dehydrated $H_4PVMo_{11}O_{40}$ material (Figure 4b) displays a sharp single proton line from distant protons at ν_H with a line width $\Delta\nu_{1/2}^{H} = 0.55$ MHz, fresh samples give rise to broad spectral features centered at ν_H (Figure 4a). The total spread of this ^{1}H ENDOR signal of about 5 MHz is indicative of protons with substantial hf interactions of approximately $A^H \approx 5$ MHz. The intensity minimums within this broad ^{1}H ENDOR signal are caused by the well-known τ-dependent suppression effect in the Mims ENDOR experiment.[21]

The phosphorus ENDOR resonance exhibits the most striking effect upon dehydration of the HPA. Species A in fresh $H_4PVMo_{11}O_{40}$ material shows a single weak ENDOR line at the phosphorus nuclear Larmor frequency ν_P with a line width of $\Delta\nu_{1/2}^{P} = 0.12$ MHz. In Mims ENDOR experiments of species B in dehydrated samples the ^{31}P signal splits into a doublet with a spacing of about 0.41 MHz. This suggests a substantially larger ^{31}P hf coupling of the V(IV) species B in dehydrated HPA in comparison with that of species A in the parent material. It is clear, therefore, that the V(IV) ions change their position with respect to the central phosphorus atoms of the Keggin molecules during the heat-treatment of the HPA.

As the position of the ^{31}P nuclei at the center of the heteroployanions are definitely known from crystallographic data it should be possible to determine the location of the V(IV) ions in the dehydrated $H_4PVMo_{11}O_{40}$ system from the phosphorus dipolar hf coupling. Thus, in the following we will focus on orientation-selective ^{31}P ENDOR spectroscopy to determine the principal values of the phosphorus hf interaction tensor $\mathbf{A^P}$

(21) Gemperle, C.; Schweiger, A. *Chem. Rev.* **1991**, *91*, 1481.

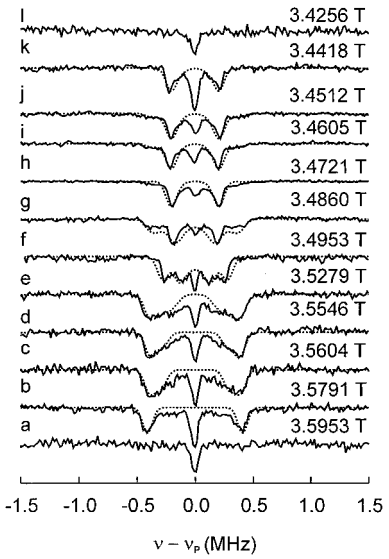

Figure 5. Experimental (solid lines) and simulated (dashed lines) W-band orientation-selective ^{31}P Mims ENDOR spectra of V(IV) ions in dehydrated $H_4PVMo_{11}O_{40}$ materials.

and its orientation with respect to the **g** tensor frame of the V(IV) ions. The orientation-selective ENDOR experiments of the V(IV) ions in dehydrated HPA materials with its axially symmetric **g** and $\mathbf{A^V}$ tensor are complicated by two facts. On one hand, the large anisotropic vanadium hf splitting into 8 lines leads to an overlapping of the $g_\perp$ ($\Theta = 90°$) and $g_{||}$ ($\Theta = 0$) spectral positions in the ESR powder patterns (Figure 3c and d). Only at W-band frequencies can the $g_\perp$ spectral region sufficiently be separated from the $g_{||}$ positions. On the other hand, the W-band field-swept ESE spectrum suffers from substantial g strain effects resulting in the smearing of the ^{51}V hf splitting (Figure 3b). This in turn diminishes drastically the resolution in the orientation-selective experiments and prevents an accurate determination of the orientation of the principal axes frame of the phosphorus hf interaction tensor with respect to the **g** tensor frame. The g strain effects are expected to have a smaller impact on orientation-selective ENDOR spectra in X-band experiments since the anisotropy of the ESR powder pattern is mainly determined by the vanadium hf coupling here. To eliminate these drawbacks orientation-selective ^{31}P ENDOR spectra have been measured at both, W- and X-band frequencies.

The W-band ENDOR spectra of V(IV) ions in dehydrated $H_4PVMo_{11}O_{40}$ are illustrated in Figure 5. The various magnetic field positions where the ENDOR spectra were taken are indicated by arrows in Figure 3b. As seen from Figure 3b,d the spectra b−k were recorded within the spectral range of the ESR powder pattern of the V(IV) species B. These ENDOR spectra reveal two signals which are symmetrically situated with respect to the phosphorus nuclear Larmor frequency ν_P. Therefore, they are assigned to ^{31}P ENDOR transitions of one phosphorus nucleus in the vicinity of the V(IV) ion belonging to the two different electron spin manifolds (weak coupling case, $2\nu_P > A^P$). In addition, all spectra show a signal at ν_P from distant ^{31}P nuclei. In spectra a and l only one signal at the phosphorus nuclear Larmor frequency is observed. It is worth mentioning that these spectra were recorded outside the spectral range of the ESR powder pattern of species B and the signal must be assigned to distant ^{31}P nuclei coupled to vanadium ions of species A.

The maximum splitting of about 0.8 MHz of the ^{31}P ENDOR signals of species B is observed in the spectrum recorded at the $g_{||}$ ($\Theta = 0$) spectral position of the ESR powder pattern

(spectrum b), whereas the minimum splitting of 0.4 MHz was obtained in spectra taken at the $g_\perp$ ($\Theta = 90°$) region (spectra h−k). The shape of the orientation-selective ENDOR spectral pattern is indicative of an axially symmetric ^{31}P hf interaction tensor $\mathbf{A^P}$ with its principal axes system orientated almost coaxial to the **g** tensor frame. Simulations of the experimental spectra were used to distinguish whether the principal values $A_{||}^P$ and $A_\perp^P$ of $\mathbf{A^P}$ have the same or different signs. The spectral simulations provided an axially symmetric phosphorus hf coupling tensor with principal values $A_{||}^P = 0.83$ MHz and $A_\perp^P = -0.44$ MHz where the $A_{||}^P$ axis approximately points along the $g_{||}$ axis of **g** tensor frame of the V(IV) ion ($\beta = 0$). However, the estimated error in the angle β between the $A_{||}^P$ and $g_{||}$ axis is $\Delta\beta = \pm 25°$ due to the large line broadening effects at W-band frequencies that are caused by g strain effects. Spectral simulations with $A_{||}^P$ and $A_\perp^P$ having different signs did not fit the experimental spectra. Especially for the spectra in Figure 5 j,k where only orientations with $\Theta > 45°$ contribute to the orientation-selective ENDOR experiments such parameter sets provide asymmetric ENDOR line shapes with wings pointing away from the phosphorus nuclear Larmor frequency ν_P. However,the wings of the asymmetric signals in these experimental spectra point toward ν_P in accordance with the different signs of the principal values of tensor $\mathbf{A^P}$ and the simulations in Figure 5. The simulations of the orientation-selective ENDOR experiments have been performed using a procedure given elsewhere.[22] The suppression effect in the Mims ENDOR experiments[21] has been taken into account in the computations. According to the chosen pulse delay $\tau = 300$ ns intensity maximums are expected to occur at $\nu_P \pm 0.85$ MHz in the ENDOR spectra and blind spots at ν_P and $\nu_P \pm 1.6$ MHz. The outer blind spots do not influence the ENDOR powder patterns significantly. However, the central blind spot at ν_P leads to a strong decrease of the ENDOR intensities in the region close to the nuclear Larmor frequency $|\nu_P - \nu| < 0.2$ for $\tau = 300$ ns where the ENDOR efficiency parameter[21] is only $F_{ENDOR} < 0.05$.

Orientation-selective ^{31}P ENDOR spectroscopy at X-band frequencies was employed to determine the orientation of the $\mathbf{A^P}$ more accurately. As already pointed out g strain effects are less serious at X-band where the anisotropy of the V(IV) powder spectra is mainly determined by the anisotropy of the vanadium hf coupling. A series of X-band ENDOR spectra were recorded in the $g_{||}$ spectral region covering a range of angles θ between 0 and 40° (spectra a−i in Figure 6). A further spectrum j was measured at the so-called "powder orientation" at $B = 0.3507$ T where most of the **g** tensor orientations contribute to the ^{31}P ENDOR signal. All spectra in Figure 6 show two groups of phosphorus ENDOR signals symmetrically situated to ν_P. The maximum splitting between the ENDOR signals of about 0.8 MHz is again observed in the spectrum taken at the $g_{||}$ ($\Theta = 0$) position in accordance with the W-band experiments. However, pronounced shoulders at the high and low-frequency wings appear in spectra that were recorded at intermediate field positions (spectra d − j) with $\Theta > 15°$. The maximum splitting between those shoulders is likewise about 0.8 MHz. This suggests that two ^{31}P hf coupling tensors denoted by $\mathbf{A^{P(I)}}$ and $\mathbf{A^{P(II)}}$ with comparable principal values but different orientations of their $A_{||}^P$ axes with respect to the $g_{||}$ axis contribute to the spectra. Moreover, two further weak signals with a splitting of 0.2−0.3 MHz were detected in the spectra a − d. These signals must be assigned to a third hf coupling tensor $\mathbf{A^{P(III)}}$ belonging to another ^{31}P nucleus. The principal values and the angles β between $A_{||}^P$ and $g_{||}$ axis of the three phosphorus hf coupling tensors were determined by spectral simulations of the experimental ENDOR spectra and are summarized in Table 2. Individual ENDOR spectra for each of the three hf tensors were computed and added to a sum spectrum which was then compared with the experimental traces. The simulated sum spectra are also displayed in Figure 6. In the simulations axially symmetric $\mathbf{A^P}$ tensors and different signs for $A_{||}^P$ and $A_\perp^P$ were used on the basis of the W-band results. Furthermore, the tensor $\mathbf{A^{P(III)}}$ was assumed to be traceless. Blind spots occur at ν_P and $\nu_P \pm 0.65$ MHz and intensity maximums at $\nu_P \pm 0.30$ MHz because of $\tau = 760$ ns. The outer blind spots are just outside the ^{31}P ENDOR signals and do again not affect the ^{31}P ENDOR powder patterns significantly. The intensity maximums at $\nu_P \pm 0.30$ MHz enhance considerably the intensity of the ^{31}P ENDOR signals at about $\nu_P \pm 0.15$ MHz which have been assigned to the third hf coupling tensor $\mathbf{A^{P(III)}}$. The corresponding ENDOR efficiency parameter $F_{ENDOR} = 0.25$ for $\tau = 760$ ns is five times higher in comparison with that for spectra measured with $\tau = 300$ ns (W-band) which explains the absence of the ^{31}P ENDOR signals belonging to the tensor $\mathbf{A^{P(III)}}$ in the W-band spectra (Figure 5).

For the given phosphorus hf coupling parameters and a proper pulse delay of $\tau = 256$ ns HYSCORE spectra are less affected

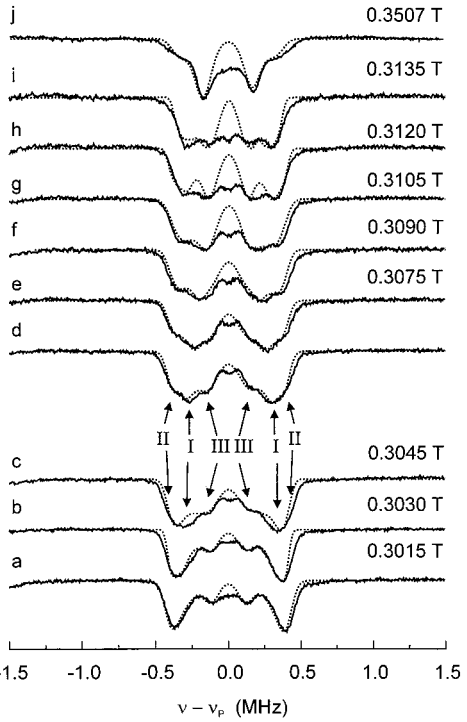

Figure 6. Experimental (solid lines) and simulated (dashed lines) X-band orientation-selective ^{31}P Mims ENDOR spectra of V(IV) ions in dehydrated $H_4PVMo_{11}O_{40}$ materials. I, II, and III label signals belong to the ^{31}P hf coupling tensors $\mathbf{A^{P(I)}}$, $\mathbf{A^{P(II)}}$, and $\mathbf{A^{P(III)}}$.

Table 2. Estimated Principal Values and Angles β between $A_{||}^P$ and $g_{||}$ Axis of the ^{31}P hf coupling tensors $A^{P(I)}$, $A^{P(ii)}$, and $A^{P(iii)}$ of V(IV) Ions in $H_4PVMo_{11}O_{40}$

tensor	$A_{||}^P$ [a] (MHz)	$A_\perp^P$ [a] (MHz)	β [b] (degree)
$\mathbf{A^{P(I)}}$	0.83	−0.44	0
$\mathbf{A^{P(II)}}$	0.83	−0.44	22
$\mathbf{A^{P(III)}}$	0.3[c]	−0.15[c]	20

[a] Estimated error is ±0.01. [b] Estimated error is ±8°. [c] A traceless tensor was assumed in the simulations.

(22) Pöppl, A.; Rudolf, T.; Manikandan, P.; Goldfarb, D. *J. Am. Chem. Soc.* in press.

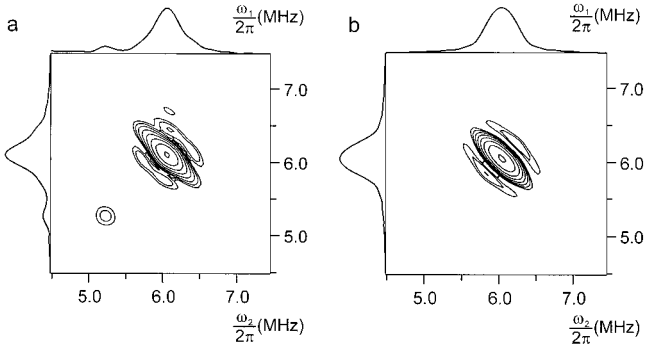

Figure 7. Experimental (a) and simulated (b) ^{31}P HYSCORE spectra of dehydrated $H_4PVMo_{11}O_{40}$ materials. The experimental spectrum was recorded at the "powder orientation" at $B = 0.3506$ T.

by suppression effects.[23] To support the analysis of the ENDOR experiment an experimental HYSCORE spectrum taken at the "powder position" of the field swept ESE spectrum B (label j in Figure 3a) of the V(IV) ion species B is presented in Figure 7a. The 2D spectrum shows a single cross-peak ridge from ^{31}P nuclei. Such cross-peak line shapes are typical for $I = {}^1/_2$ nuclei with weak dipolar hf couplings.[24] It seems worth noting that in general two cross-peak ridges are expected to occur in HYSCORE spectra of $I = {}^1/_2$ nuclei in disordered systems, but in cases of weak dipolar hf couplings and negligible isotropic hf interactions the two ridges overlap and cannot be resolved in the 2D experiment. The diagonal peak at (5.2; 5.2) MHz is an experimental artifact. Two more ridges with lower intensity are observed symmetrically to the ^{31}P cross-peak ridge. They are caused by wiggles after 2D FT, because no apodization of the time domain data was applied to avoid additional line broadening effects in the 2D spectrum. A simulation of the ^{31}P HYSCORE spectrum (Figure 7b) using the phosphorus hf interaction parameters in Table 2 is in good agreement with experimental 2D spectrum and supports the ENDOR results. In the simulation individual HYSCORE spectra for the three tensors $\mathbf{A^{P(I)}}$, $\mathbf{A^{P(II)}}$, and $\mathbf{A^{P(III)}}$ are computed as described elsewhere[25] and finally added to the resulting 2D spectrum.

5. Discussion

The obtained spin Hamiltonian parameters of the V(IV) ions in fresh and dehydrated (calcined) $H_4PVMo_{11}O_{40}$ materials (Table 1) are in good accordance with previously published ESR results on heteropolyacids.[8−12] On the basis of the vanadium **g** tensor and hf interaction parameters it was concluded that paramagnetic vanadium ions exist as vanadyl (VO^{2+}) species in both hydrated and dehydrated HPA materials (with different concentration[12]). However, conclusive experimental evidence about the nature of the VO^{2+} ions and their location in the heteropolyacids could not be derived from conventional ESR experiments. Such information can be gained for the first time from the analysis of the ^{31}P ENDOR results as shown below.

Hydrated HPA. For the fresh material the reasonable suggestion was given by Bayer et al.[10] and Lee et al.[12] that VO^{2+} ions are coordinated to crystallization water molecules resulting in vanadyl pentaaqua complexes $[VO(H_2O)_5]^{2+}$. The complexes are expected to be located in the void space of the secondary structure between the heteropolyanions. The ENDOR results on the fresh $H_4PVMo_{11}O_{40}$ sample support this assumption where species A is assigned to $[VO(H_2O)_5]^{2+}$ complexes. Even without a detailed analysis of the proton ENDOR signals from fresh HPA materials the observed strong ^{1}H hf couplings of about $A^H \approx 5$ MHz (Figure 4a) indicate the direct coordination of water molecules to the VO^{2+} species. Indeed ^{1}H hf couplings of this magnitude have been found for $[VO(H_2O)_5]^{2+}$ complexes in various matrixes.[26] The location of the $[VO(H_2O)_5]^{2+}$ complex can be deduced from the phosphorus ENDOR signal in Figure 4a. The spectrum shows only a single ^{31}P ENDOR resonance at ν_P from distant phosphorus nuclei. The line width $\Delta\nu^{P}_{1/2} = 0.12$ MHz of this signal corresponds to a maximum dipolar hf coupling between the phosphorus nuclei and the vanadyl complex of approximately $T^{P}_{max} \approx 0.1$ MHz which in turn yields a minimum distance between the vanadium ion and the weakly coupled ^{31}P nuclei of $r_{V-P} \approx 0.68$ nm. Taking into account the diameter of the heteropolyanion of about 1.04 nm[27] the $[VO(H_2O)_5]^{2+}$ complexes in the parent HPA materials must actually be located in the void space of the secondary structure between the heteropolyanions.

Anhydrous HPA. The principal values of the **g** and vanadium hf coupling tensor of the vanadyl species B in dehydrated HPA materials differ significantly from those of the $[VO(H_2O)_5]^{2+}$ complex (species A) observed in the parent sample (Table 1). This implies that the VO^{2+} coordination is changed upon heat treatment (calcination) of the HPA. The most likely scenario is a loss of the coordinated crystallization water molecules in the anhydrous material and the subsequent coordination of the vanadyl species B to outer oxygen atoms of the heteropolyanions.[8] For instance, Bayer et al.[10] suggested for the dehydrated $[VO(H_2O)_5]H[PMo_{12}O_{40}]$ system, where the vanadyl ions are counterions of the heteropolyanions, that the VO^{2+} species is coordinated to four terminal oxygens O(4) each from different Keggin molecules to bridge the four $[PMo_{12}O_{40}]^{-3}$ anions.

The loss of the coordinated water molecules for species B is evident from the ENDOR spectrum of the dehydrated $H_4PVMo_{11}O_{40}$ material in Figure 4b. In comparison with the fresh HPA the hf interactions with strongly coupled protons from directly coordinated water molecules are not observed in the ENDOR spectrum of species B. The detected single ENDOR line at ν_H is due to weakly coupled distant protons which might presumably be assigned to the Brønsted acid protons[15] bound to the bridging oxygen atoms O(2) and O(3) of the heteropolyanions. From the line width $\Delta\nu^{H}_{1/2} = 0.55$ MHz of this ^{1}H ENDOR signal we can again roughly estimate a maximum dipolar proton hf interaction of approximately $T^{H}_{max} \approx 0.5$ MHz corresponding to a minimum VO^{2+}-H distance of about $r_{V-H} \approx 0.54$ nm.

The position of the VO^{2+} species B can be deduced from the determined phosphorus hf interaction tensors $\mathbf{A^{P(I)}}$ and $\mathbf{A^{P(II)}}$ given in Table 2. Both tensors provide a small isotropic hf coupling of $A^{P(I,II)}_{iso} = -0.02$ MHz and principal values $T^{P(I,II)}_{xx} = T^{P(I,II)}_{yy} = -0.42$ MHz, $T^{P(I,II)}_{zz} = 0.85$ MHz of the ^{31}P dipolar hf coupling tensor $\mathbf{T^P}$. The negligible values $A^{P(I,II)}_{iso}$ justifies to determine a distance $r_{V-P} = 0.42$ (±0.02) nm between the VO^{2+} ion and the central phosphorus atom of the Keggin structure using the point dipole approximation. The vector joining the P and V atoms which is defined by the *z* axis of the $\mathbf{T^P}$ tensor points exactly along the $g_{||}$ axis given by the V=O bond direction of the vanadyl complex for the tensor $\mathbf{A^{P(I)}}$. In the case of $\mathbf{A^{P(II)}}$ a small tilt angle of $\beta = 22°$ between the V−P

(23) Höfer, P. *J. Magn. Reson. A* **1994**, *111*, 77.
(24) Pöppl, A, Kevan, L. *J. Phys. Chem.* **1996**, *100*, 3387.
(25) Pöppl, A.; Hartmann, M.; Böhlmann, W.; Böttcher, R. *J. Phys. Chem. A* **1998**, *102*, 3599.
(26) Van Willigen, H. *J. Magn. Reson.* **1980**, *37*, 37. (b) Atherton, N. M.; Shackleton, J. F. *Mol. Phys.* **1980**, *39*, 1471. (c) Kevan, L. *J. Phys. Chem.* **1984**, *88*, 327. (d) Tyryshkin, A. M.; Dikanov, S. A.; Goldfarb, D. *J. Magn. Reson. A* **1993**, *105*, 271.
(27) D'Amour, H.; Allman, R. *Z. Kristallogr.* **1976**, *143*, 1.

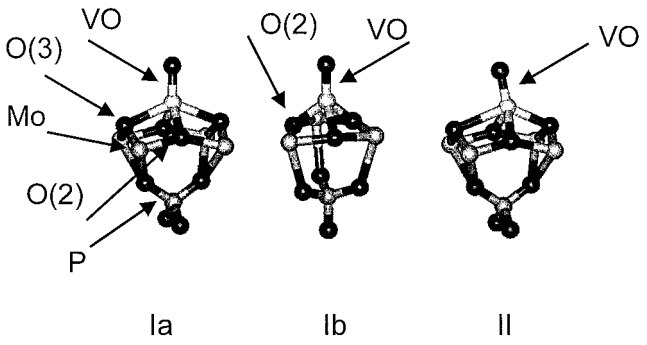

Figure 8. Schematic drawings of the proposed vanadyl complexes in dehydrated (calcined) $H_4PVMo_{11}O_{40}$ materials: (structure Ia) coordination of the VO^{2+} to four oxygen atoms O(2) and O(3) in a distorted square-pyramidal coordination geometry, (structure Ib) coordination of the VO^{2+} to three oxygen atoms O(2) in a trigonal-pyramidal coordination geometry, and (structure II) VO^{2+} coordination to four oxygen atoms O(2) and O(3) with equalized bond distances to three oxygens.

direction and the V=O bond axis is obtained. On the basis of the orientation of the $\mathbf{T^P}$ tensors we must reject the assumption of Bayer et al.[10] where the vanadyl species is coordinated to four terminal oxygens from surrounding Keggin molecules in the dehydrated (calcined) HPA. Such a VO^{2+} species would imply a square-pyramidal coordination geometry with the V=O bond directed along the 4-fold rotation axis and the O(4) oxygens from the four heteropolyanions at the base of the pyramid. For such a complex structure the *z* axis of the $\mathbf{T^P}$ tensor is not expected to point along the V=O bond but should be approximately orientated parallel to the base of the pyramid. The maximum dipolar hf couplings would then be observed in orientation-selective ENDOR spectra recorded close to the $g_\perp$ position ($\theta \approx 90°$) in obvious contradiction with the experimental results. Another likely position of the VO^{2+} ion might be a molybdenum site in the $PVMo_{11}O_{40}^{-4}$ anion, but the distance $\boldsymbol{r}_{V-P} = 0.42$ nm has to be compared with the P−Mo distances of 0.35 nm[27] in the heteropolyanion molecule. Thus we can also exclude the incorporation of paramagnetic VO^{2+} species at Mo sites in the anhydrous acid.

On the basis of the ^{31}P ENDOR results we deduce that the VO^{2+} ion in dehydrated $H_4PVMo_{11}O_{40}$ materials is attached to the outer surface of the heteropolyanions and coordinates to the bridging oxygens O(2) and O(3). The obtained two phosphorus hf coupling tensors $\mathbf{A^{P(I)}}$ and $\mathbf{A^{P(II)}}$ indicate that VO^{2+} complexes with two different structures exist in the dehydrated materials.

For the tensor $\mathbf{A^{P(I)}}$ having $\beta = 0$ two possible complex structures Ia and Ib are in accordance with the ENDOR results. Schematic drawings of the two complex structures are depicted in Figure 8. In structure Ia the vanadyl ion coordinates to two outer bridging oxygens O(2) and two oxygens O(3) from the heteropolyanion with a slightly distorted square-pyramidal coordination geometry whereas for the second structure Ib the VO^{2+} ion is coordinated to three oxygens O(2) in a trigonal-pyramidal coordination geometry. In both coordination geometries the vanadyl oxygen is at the apex of the pyramid, pointing away from the $PVMo_{11}O_{40}^{-4}$ anion. For both complex geometries the V=O bond direction is expected to be approximately directed along a vector joining the P and V atom ($\beta = 0$) in accordance with the orientation of the *z* axis of the $\mathbf{T^P}$ tensors. From the crystallographic positions of the atoms O(2) and O(3) in the heteropolyanion[27] and the determined V−P distance $\boldsymbol{r}_{V-P} = 0.42$ nm we calculate for the complex structure Ia vanadium − oxygen distances $\boldsymbol{r}_{V-O(2)} = 0.21$ nm and $\boldsymbol{r}_{V-O(3)} = 0.23$ nm and bond angles β_{bond} of 128° and 113° between the V=O bond direction and the V−O(2) and V−O(3) bonds, respectively. The trigonal-pyramidal complex geometry Ib gives $\boldsymbol{r}_{V-O(2)} = 0.19$ nm and $\beta_{bond} = 128°$. Therefore, the vanadium ion is located in an off-plane position from the base of the pyramidal complexes in both structures. The estimated bond distances and bond angles compare well with data from other VO^{2+} complexes.[26,28] However we cannot distinguish between the two proposed complex geometries on the basis of the ^{31}P ENDOR results.

A deviation of the *z* axis of $\beta = 22°$ from the vector joining the P and V atom is obtained for the tensor $\mathbf{A^{P(II)}}$. This implies that the VO^{2+} ion is likewise coordinated to two oxygens O(2) and two oxygens O(3). But the vanadyl ion is slightly shifted from the center of gravity of the four oxygens to equalize the bond distance to three of those four oxygen atoms (structure II in Figure 8). For $\boldsymbol{r}_{V-P} = 0.42$ nm and V−O bond distances $\boldsymbol{r}_{V-O(2)} = \boldsymbol{r}_{V-O(3)} = 0.20$ nm we obtain $\beta_{bond} = 126°$ and $\beta = 20°$ in good accordance with the orientation of the tensor $\mathbf{A^{P(II)}}$. The distance between the vanadium and the fourth oxygen O(3) is then $\boldsymbol{r}_{V-O(3)} = 0.25$ nm.

The third phosphorus hf interaction tensor $\mathbf{A^{P(III)}}$ is assigned to P atoms from neighboring Keggin molecules. Assuming a purely dipolar hf coupling we calculate a distance of about 0.6 nm between the VO^{2+} complex and the central phosphorus atom of the neighboring heteropolyanion. This seems to be a reasonable estimate when we take into account the diameter of the $PVMo_{11}O_{40}^{-4}$ anion of 1.04 nm.[27]

6. Conclusions

The location of the paramagnetic V(IV) ions in hydrated and dehydrated (anhydrous, calcined) $H_4PVMo_{11}O_{40}$ materials could be determined by orientation-selective pulsed ENDOR and HYSCORE spectroscopy. Vanadyl species are not found to be incorporated at molybdenum sites into the Keggin structure of the HPA in either fresh nor dehydrated samples. In the parent material the paramagnetic vanadium species exist as vanadyl pentaaqua complexes $[VO(H_2O)_5]^{2+}$ located in the void space between the heteropolyanions. Upon dehydration the $[VO(H_2O)_5]^{2+}$ complexes lose the coordinated crystallization water molecules and the VO^{2+} species are directly bound to the Keggin molecules in the dehydrated HPA. Distorted square-pyramidal and trigonal-pyramidal VO^{2+} complexes evolve with the V(IV) ion coordinated to four or three bridging oxygen atoms of one $PVMo_{11}O_{40}^{-4}$ anion, respectively. These coordination geometries result in a distance of 0.42 nm between the vanadyl ion and the central phosphorus atom of the Keggin molecule where the vanadyl oxygen bond points away from the heteropolyanion. It seems justified to speculate that these exposed vanadyl species at the surface of the heteropolyanions might be involved in the catalytic cycle of selective oxidation reactions. This result has to be taken into account for the necessary reevaluation of the role of vanadium in the catalytic system. On the basis of the determined complex structures we may conclude that the VO^{2+} complexes do not act as bridges in the secondary structure between neighbored heteropolyanions in the dehydrated $H_4PVMo_{11}O_{40}$ system.

Finally we have to emphasize that in the case of the anhydrous material it was possible to completely analyze the hf coupling tensor including its orientation of a phosphorus nucleus in the fourth coordination sphere around the V(IV) ion from powder ENDOR experiments. This demonstrates the potential of combined orientation-selective pulsed ENDOR spectroscopy at

(28) Ballhausen, C. J.; Djurinskij, B. F.; Watso, K. J. *J. Am. Chem. Soc.* **1968**, *90*, 3305.

X- and W-band frequencies for the investigation of paramagnetic transition metal ion complexes in disordered systems.

Acknowledgment. This research was supported by the Deutsche Forschungsgemeinschaft within the Schwerpunktprogramm "Hochfeld EPR-Spektroskopie". The authors thank Professor R. Schlögl (Fritz Haber Institute Berlin, Germany) for helpful discussions.

JA004291N